LEGIBILITY NOTICE

A major purpose of the Technical Information Center is to provide the broadest dissemination possible of information contained in DOE's Research and Development Reports to business, industry, the academic community, and federal, state and local governments.

Although a small portion of this report is not reproducible, it is being made available to expedite the availability of information on the research discussed herein.

ornl

ORNL/TM-9888

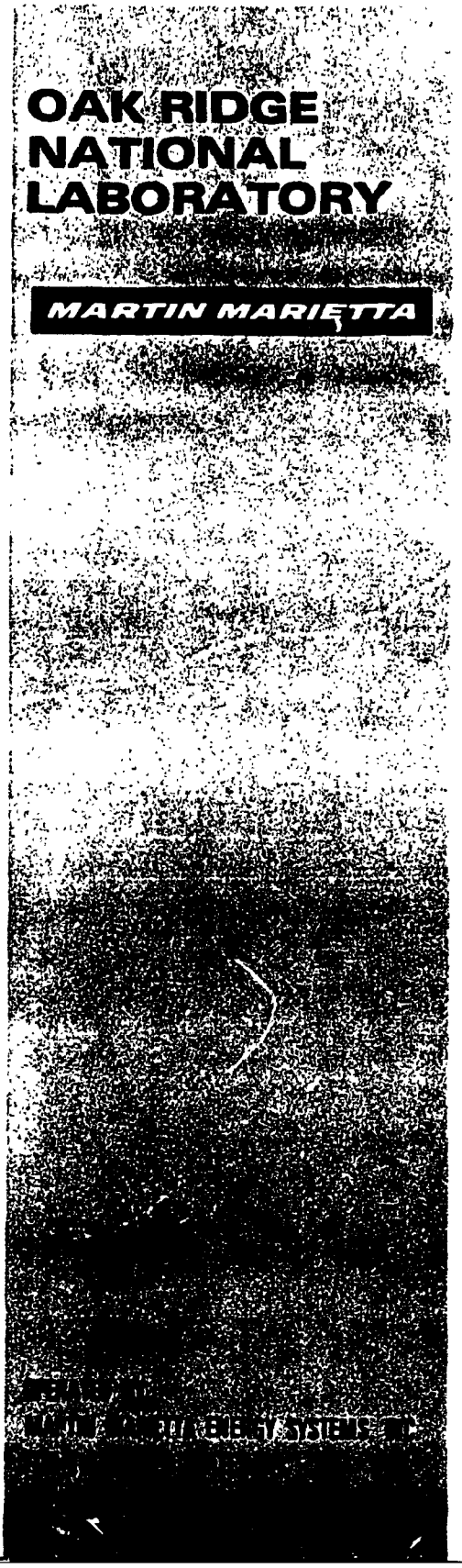

Comparisons of Calculated and Measured Spectral Distributions of Neutrons From a 14-MeV Neutron Source Inside the Tokamak Fusion Test Reactor

R. T. Santoro
J. M. Barnes
R. G. Alsmiller, Jr.
M. B. Emmett
J. D. Drischler

ORNL/TM-9888
Distribution Category UC-20d

ORNL/TM--9888

Engineering Physics and Mathematics Division

DE86 006774

Comparisons of Calculated and Measured Spectral Distributions of Neutrons from a 14-MeV Neutron Source Inside the Tokamak Fusion Test Reactor*

R. T. Santoro, J. M. Barnes,+ R. G. Alsmiller, Jr.
M. B. Emmett,+ and J. D. Drischler

*Submitted for Journal publication
+Computing & Telecommunications

Date of Issue: December 1985

Research sponsored by
Office of Fusion Energy
U.S. Department of Energy

Prepared by the
Oak Ridge National Laboratory
Oak Ridge, Tennessee 37831
operated by
Martin Marietta Energy Systems, Inc.
for the
U.S. DEPARTMENT OF ENERGY
under Contract No. DE-AC05-840R21400

ACKNOWLEDGMENT

The authors gratefully acknowledge many helpful discussions with J. K. Dickens concerning the experimental data.

TABLE OF CONTENTS

I. INTRODUCTION

Fusion reactors will, of necessity, have very complex geometric configurations and because of this complexity and the high-energy (~14 MeV) neutrons involved there is some question as to whether state-of-the-art radiation transport methods are adequate for the design of the shielding and blankets for such reactors.

The Tokamak Fusion Test Reactor (TFTR)[1] being constructed at the Princeton Plasma Physics Laboratory will not have a blanket, but it will have much of the complexity, e.g., toroidal and poloidal coils, of a fusion reactor. Deuterium–tritium operation, i.e., 14-MeV neutron production, at the TFTR is still in the future. Recently, however, a series of measurements were made of the neutron spectral distributions (energy $\geq$0.91 MeV) around the TFTR from a point source of 14-MeV neutrons inside the TFTR vacuum vessel.[2] In the present paper calculated results of neutron spectra carried out using Monte Carlo methods (MORSE[3]) and a realistic model of the TFTR are presented and compared with experimental data.

In Section II the method of calculation is described, and in Section III the comparisons between calculated and experimental data are presented and discussed.

II. METHOD OF CALCULATION

A. Geometry and Materials

The TFTR was modeled in considerable detail using the combinatorial geometry routines that are contained in the MORSE[3] code system. The dimensions used in the modeling were taken from Ref. 1.

In Fig. 1 four diagrams of the TFTR model that was used in the calculations are shown. The material of the various elements in the diagrams is also specified in the diagrams. These diagrams were drawn from the MORSE code geometry input using the code JUNEBUG-II.[4] The four diagrams are shown separately for clarity, but it is to be understood that they are superimposed in the complete model. The central column shown in each diagram is the basis of the superposition. Figure 1A shows, in addition to the central column, the toroidal vacuum vessel and the concrete machine support. The concrete machine support contains a variety of holes into the basement (not shown) of the test facility. In Fig. 1B the toroidal field coils are shown. In Fig. 1C the poloidal field coils are shown, and in Fig. 1D the umbrella structure and the machine support columns are shown. The concrete in the support columns (see Fig. 1D) has a cross-sectional area of 0.20 m by 0.52 m. In addition to the structural elements shown in Fig. 1, the calculational model also includes the concrete (ordinary) floor (thickness = 1.22 m) that separates the test cell from the basement, the walls and roof of the test cell, and the walls and floor of the test cell basement. The test cell has a cross-sectional area of 35 m by 43 m and a height of 7.1 m. The roof and walls of the test cell are made of ordinary concrete and have thicknesses of 1.2 m. The distance from the test cell floor to the concrete basement floor is 5.48 m. Finally, in the calculations the test cell was assumed to be filled with air. The atomic compositions of all of the materials used in the calculations were taken from the work of Long-Poe Ku[5] and are given in Table 1.

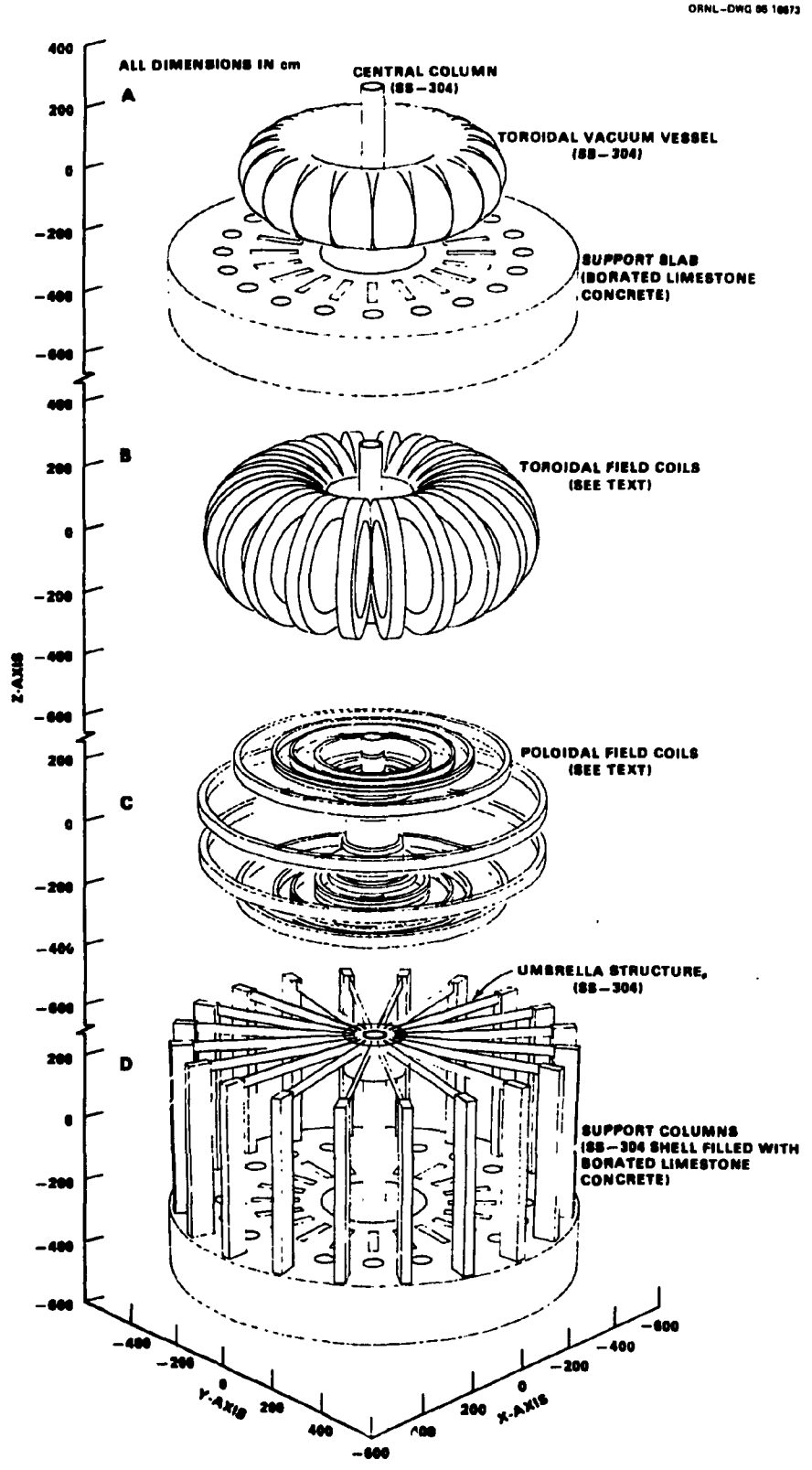

Fig. 1. Schematic diagrams of the TFTR model used in the calculations. The four diagrams must be superimposed to obtain the actual model used. Also several elements, wall, roof, floor, etc., that were included in the calculations (see Section II.B) are not shown.

Table 1

Composition of Materials Used in the Calculations

	Number Densities [Atom/cm × barn]					
Element	**SS-304**	**Borated Limestone Concrete**	**Ordinary Concrete**	**Toroidal Field Coil**	**Poloidal Field Coil**	**Air**
H		8.25×10^{-3}	7.83×10^{-3}	2.64×10^{-3}	4.40×10^{-3}	
B		1.09×10^{-3}		2.06×10^{-4}	3.42×10^{-4}	
C		1.05×10^{-2}		1.10×10^{-3}	1.84×10^{-3}	
N						4.20×10^{-5}
O		4.32×10^{-2}	4.38×10^{-2}	3.00×10^{-3}	5.00×10^{-3}	1.13×10^{-5}
Na		1.31×10^{-5}	1.05×10^{-3}			
Mg		1.88×10^{-4}	1.49×10^{-4}			
Al		2.63×10^{-4}	2.39×10^{-3}	1.40×10^{-4}	2.34×10^{-4}	
Si		1.09×10^{-3}	1.58×10^{-3}	1.37×10^{-3}	1.18×10^{-3}	
S			5.64×10^{-5}			
A						2.54×10^{-7}
K		1.39×10^{-5}	6.93×10^{-4}			
Ca		1.31×10^{-5}	2.92×10^{-3}	2.53×10^{-4}	4.21×10^{-4}	
Cr	1.74×10^{-2}			6.46×10^{-3}		
Mn	1.19×10^{-3}			4.42×10^{-3}		
Fe	6.13×10^{-2}	1.50×10^{-4}	3.13×10^{-4}	2.17×10^{-2}		
Co						
Ni	6.79×10^{-3}			9.54×10^{-4}		
Cu				4.33×10^{-2}	7.21×10^{-2}	
Ba		1.24×10^{-4}				

B. Transport Calculations

All of the transport calculations were carried out using MORSE[3] and the FLUNG[6] multigroup cross-section library that is based on ENDF/B-IV. Only neutron transport at energies greater than 0.91 MeV is considered here since this is the lowest energy neutron that was considered in the experiments. The experiments did include measurements of photon spectra but these spectra are not considered here.

Experimentally the neutron source was provided by a D-T generator that was placed inside the TFTR vacuum vessel. In the calculations the source neutrons were assumed to emanate isotropically from a point. That is, the small measured anisotropy in the source neutrons was neglected in the calculations.[2] The measured anisotropy does not include, because of the generator structure, measurements at the very back angles and these angles are involved in at least one of the experiments (see discussion of Exp. 5 at the end of Section III). The source neutrons in the calculations were taken to be in the group between 13.5 to 14.9 MeV.

The position of the source and the detector with respect to the TFTR geometry varied with the experiments (see below). To improve the statistical accuracy of the calculations the neutron source was biased, and the particles weighted appropriately, so that 90% of the neutrons were emitted uniformly into a cone of half-angle 15° about the line joining the source and the detector.

C. Experimental Data and Details of Obtaining Calculated Results for Comparison with the Experimental Data

In Fig. 2 a schematic of the TFTR test cell as it existed at the time of the experiments is shown. The neutral beam injector, the horizontal limiter, the tokamak vacuum pumping system, and the x-ray experimental setup were present during the experiments but were not included in the calculational model. The points P1 to P5 in Fig. 2 represent the source positions for what will hereinafter be termed Exps. 1 to 5. The positions P1 to P5 are located at the center of the toroidal vacuum vessel (radius 2.65 m). If north is taken to be 0°, then the points P1 to P5 are located with respect to the center of the central column at angles of 0°, 36°, 72°, 108°, and 180°. Again, taking 0° to be north, the direction of the deuteron beam in the D-T generator in Exps. 1 to 5 is 90°, 126°, 162°, 128°, and 270°, respectively. The direction of the deuteron beam does not enter into the calculations since the neutron source is assumed to be isotropic. In Exps. 1, 3, 4, and 5 the detector was located at position D1 (radius = 8.85 m, angle = 117.8°) and in experiment 2 the detector was at position D2 (radius = 4.37 m, angle = 108.0°). The source positions and the detector positions are located in the same horizontal plane. Measurements were also made for source positions other than those shown in Fig. 2, but these additional experiments are not considered here.

The experimental data presented in Ref. 2 are the unfolded neutron fluence spectra at the position of the detectors. The number of source neutrons that were emitted during each of the experiments was measured independently, and the results are given in Table 2. The calculated results that are compared with the experimental fluence spectra in Section III have been normalized to the number of source neutrons given in Table 2.

ORNL DWG 83-17016R

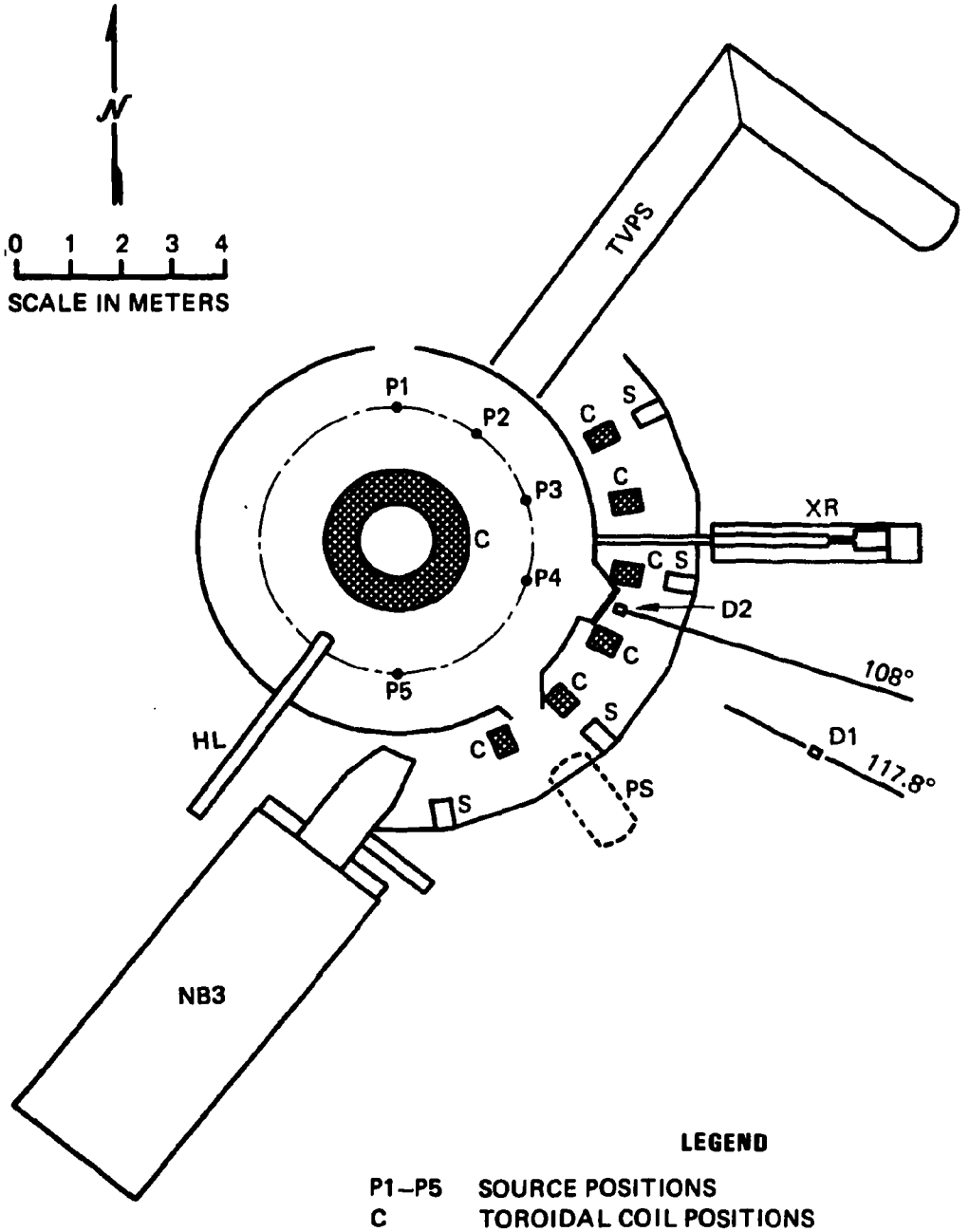

Fig. 2. Schematic of the test cell floor at the time of the experiment showing the source and detector positions used in the experiments.

Table 2

Measured Number of Source Neutrons in Each of the Experiments

Exp.	No. of Source Neutrons
1	$(4.21 \pm 0.25) \times 10^{11}$
2	$(2.78 \pm 0.17) \times 10^{11}$
3	$(4.66 \pm 0.28) \times 10^{11}$
4	$(3.20 \pm 0.19) \times 10^{11}$
5	$(6.03 \pm 0.30) \times 10^{11}$

To obtain calculated results that are directly comparable with the experimental fluence spectra, it was necessary to convolute the calculated neutron fluence per unit energy with the energy resolution of the detector used in the measurements. In accordance with Ref. 2, the response function was assumed to be Gaussian with a resolution determined by

$$R = \frac{E}{100}\sqrt{30 + \frac{1000}{E}} \quad , \tag{1}$$

where

R = full width at half-maximum in MeV,
E = neutron energy in MeV.

III. RESULTS AND DISCUSSION

In Figs. 3–7 the experimental and calculated neutron fluences per unit energy at energies ≥0.91 MeV are compared for Exps. 1 to 5, respectively. Note that in Figs. 3–7 the experiments are presented in the order Exp. 2, Exp. 4, Exp. 3, Exp. 1, and Exp. 5, since this is the order in which it will be convenient to discuss them. In Figs. 3–7 the crosshatched region represents the 68% confidence interval in the experimental measurements and the solid curves represent plus and minus one standard deviation of the statistical error in the calculations.

Table 3 shows the measured and calculated fluences of neutrons with energy ≥0.91 MeV obtained from the data shown in Figs. 3–7. The uncertainties in the neutron fluences in Table 3 were obtained assuming uncorrelated data. Also given in Table 3 are the ratios of the calculated to measured fluences.

Experiment 2, for which the source is at the point P2 and the detector is at the point D2 in Fig. 2, will be considered first. In this experiment there is only a small amount of material on a direct line between the source and the detector and thus the details of the TFTR geometry are not expected to have as significant an effect on the results as in the experiments discussed below. In other words, this experiment is considered first because it is thought to provide the least challenge to the calculational procedures. In Fig. 3 the calculated results are in substantial agreement with the experimental data at energies below approximately 13 MeV and overestimate slightly the high-energy peak above 13 MeV. In Table 3 the ratio of the calculated to the experimental fluence at energies ≥0.91 MeV for Exp. 2 is only moderately larger than unity so the calculated results reproduce the experimental data quite well in both shape and magnitude.

Experiment 4, for which the source is at P4 and the detector is at D1 in Fig. 2, will be considered next. In this experiment a direct line between the source and the detector passes through a toroidal field coil. Nevertheless, the position of the source and detector are such that the results in this experiment are expected to be only moderately dependent

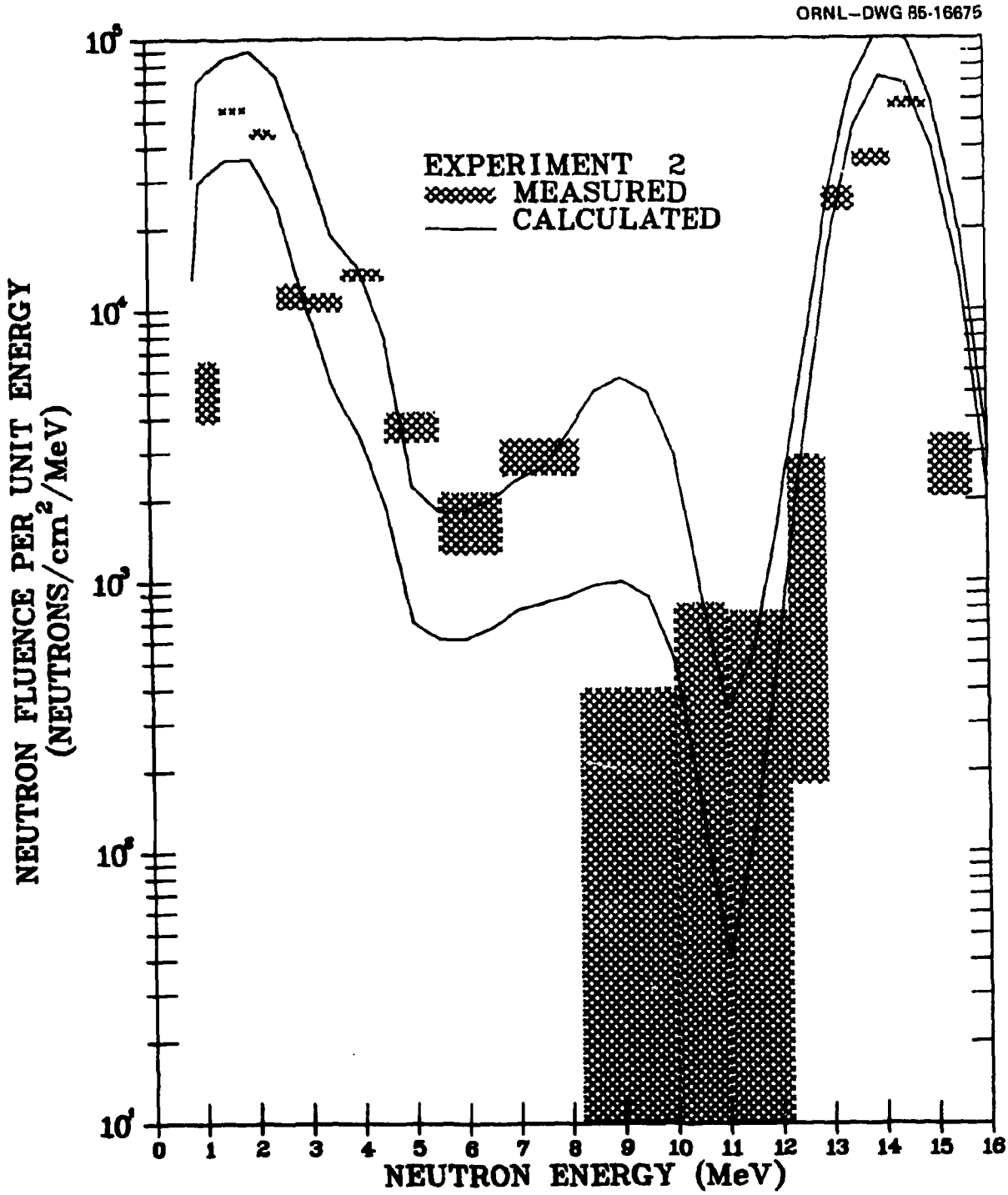

Fig. 3. Comparison of measured and calculated neutron fluences per unit energy for Exp. 2. The crosshatched regions indicate the 68% confidence intervals in the experimental measurements and the solid lines indicate the upper and lower bounds (± one standard deviation) due to the statistical error in the calculations .

Table 3

Comparisons of Calculated and Measured Neutron Fluences

Experiment No.	Fluence of Neutrons With Energy ≥0.91 MeV [Neu. cm^{-2}]		Ratio of Calculated to Measured Fluence (≥0.91 MeV)
	Measured	Calculated	
1	$4.4\times10^{3}\pm4.2\times10^{2}$	$1.5\times10^{4}\pm1.4\times10^{3}$	3.4 ± 0.5
2	$1.8\times10^{5}\pm3.7\times10^{3}$	$3.2\times10^{5}\pm2.7\times10^{4}$	1.8 ± 0.2
3	$1.4\times10^{4}\pm6.5\times10^{2}$	$3.2\times10^{4}\pm2.0\times10^{3}$	2.3 ± 0.2
4	$3.2\times10^{4}\pm1.3\times10^{3}$	$5.7\times10^{4}\pm5.5\times10^{3}$	1.8 ± 0.2
5	$1.3\times10^{4}\pm4.3\times10^{2}$	$3.8\times10^{4}\pm2.3\times10^{3}$	2.9 ± 0.2

on the details of the TFTR geometry. In other words, this experiment is expected to provide more of a challenge to the calculational procedures than Exp. 2, but less than the experiments discussed below. In Fig. 4 the calculated results are in substantial agreement with the experimental data at all energies considered. In Table 3 the ratio of the calculated to the experimental fluences for Exp. 4 is, as it is for Exp. 2, only moderately larger than unity, so again the calculated results reproduce the experimental data quite well both in shape and magnitude.

Experiment 3, for which the source is at position P3 and the detector is at position D1 in Fig. 2, will be considered next. The details of the TFTR geometry should, in this case, enter significantly in determining the experimental results. To illustrate this it may be noted that the uncollided fluence at the position of the 1 cm^2 detector is approximately 2×10^5 while the measured fluence at energies $\geq$12.9 MeV is approximately 5×10^3, so the experimental data indicate that there has been a substantial attenuation of the source neutrons. In Fig. 5, the calculated fluence per unit energy overestimates the experimental data at low energies ($\leq$6 MeV) and underestimates the experimental data at the higher energies ($\geq$10 MeV). In particular, the calculations underestimate the peak in the vicinity of the source energy by approximately a factor of 4 and show a high-energy peak in the 13- to 14-MeV region rather than in the 14- to 15-MeV region. Of all of the experiments considered here, it is only in this experiment that there is substantial disagreement in shape at the higher energies between the calculated and experimental data. In Table 3 the ratio of the calculated to experimental fluence for Exp. 3 is 2.3 $\pm$ 0.2, which is not unreasonable for an absolute comparison in such a complicated geometry.

The comparison of the calculated and measured fluence per unit energy for Exp. 1 is shown in Fig. 6. In this experiment the source was at position P1 and the detector was at position D1. The uncollided fluence at the position of the detector is $\sim1\times10^5$ and the measured fluence $\geq$12.9 MeV is $\sim2\times10^3$ so in this experiment, as in Exp. 3, substantial attenuation of the source neutrons is indicated. In Fig. 6 the calculated results are significantly larger than the experimental data at energies $\leq$4 MeV, but at the higher energies, and in particular in the vicinity of the source energy, the experimental and calculated fluences per unit energy are in very good agreement. There is no known reason why the agreement at the higher energies should be better in Exp. 1 than it was in Exp. 3, but presumably geometric uncertainties were more crucial in Exp. 3 than in Exp. 1. In Table 3 the ratio of the calculated to the measured fluence is larger than in the experiments considered previously because of the overestimation by the calculation of the fluence at the lower energies.

The calculated and experimental fluences per unit energy for Exp. 5 are compared in Fig. 7. This experiment is somewhat different than the other experiments in that the beam direction, i.e., the direction of the accelerated deuteron beam with respect to north, is 270° so that the source neutrons that are directed from source position P5 to the detector at position D1 are those neutrons that are emitted at very back angles with respect to the direction of the deuteron beam. Thus, the source neutron anisotropy due to the presence of the *D-T* generator structure should have the most pronounced effect in this experiment.

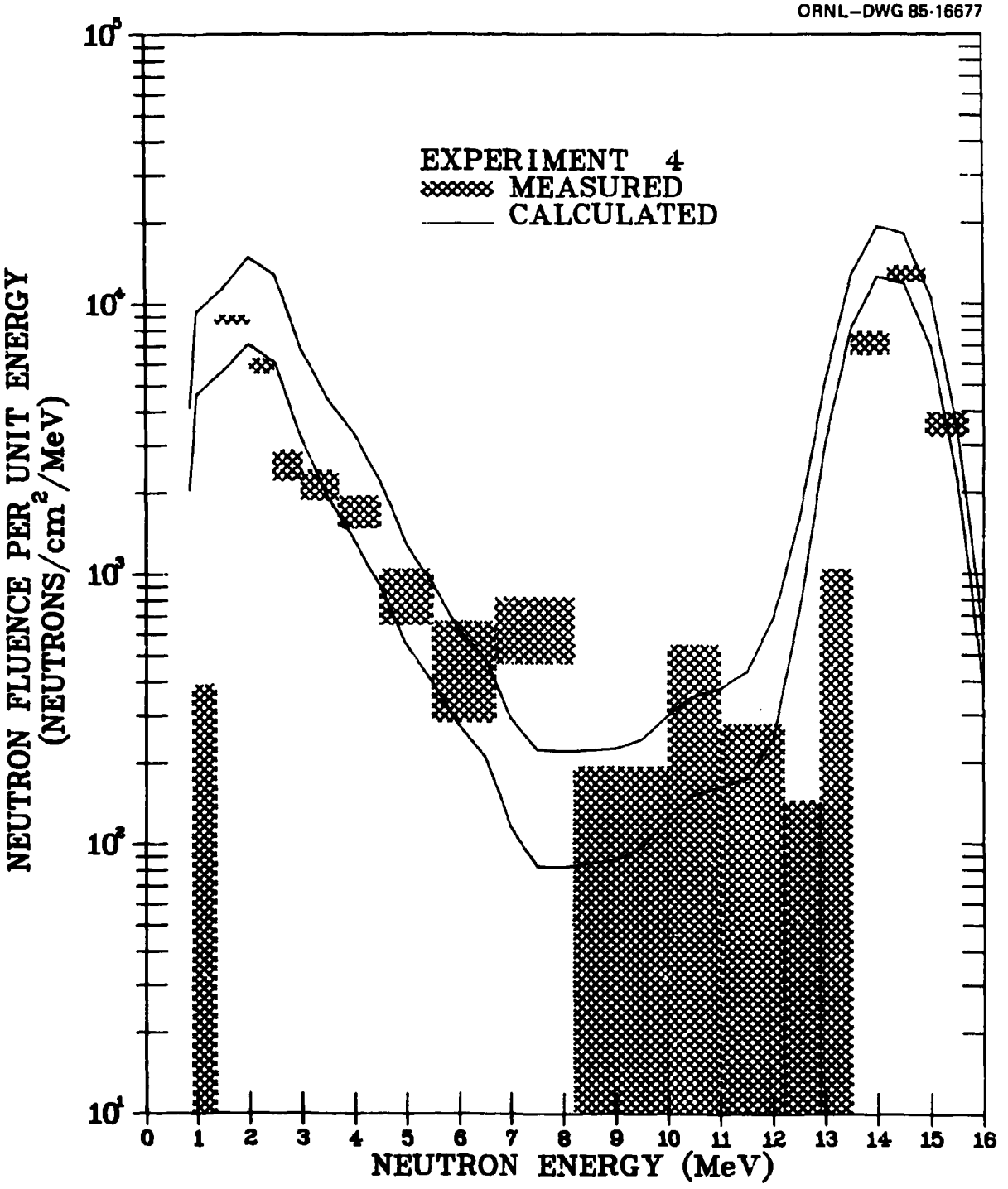

Fig. 4. Comparison of measured and calculated neutron fluences per unit energy for Exp. 4. The crosshatched regions indicate the 68% confidence intervals in the experimental measurements and the solid lines indicate the upper and lower bounds (± one standard deviation) due to the statistical error in the calculations .

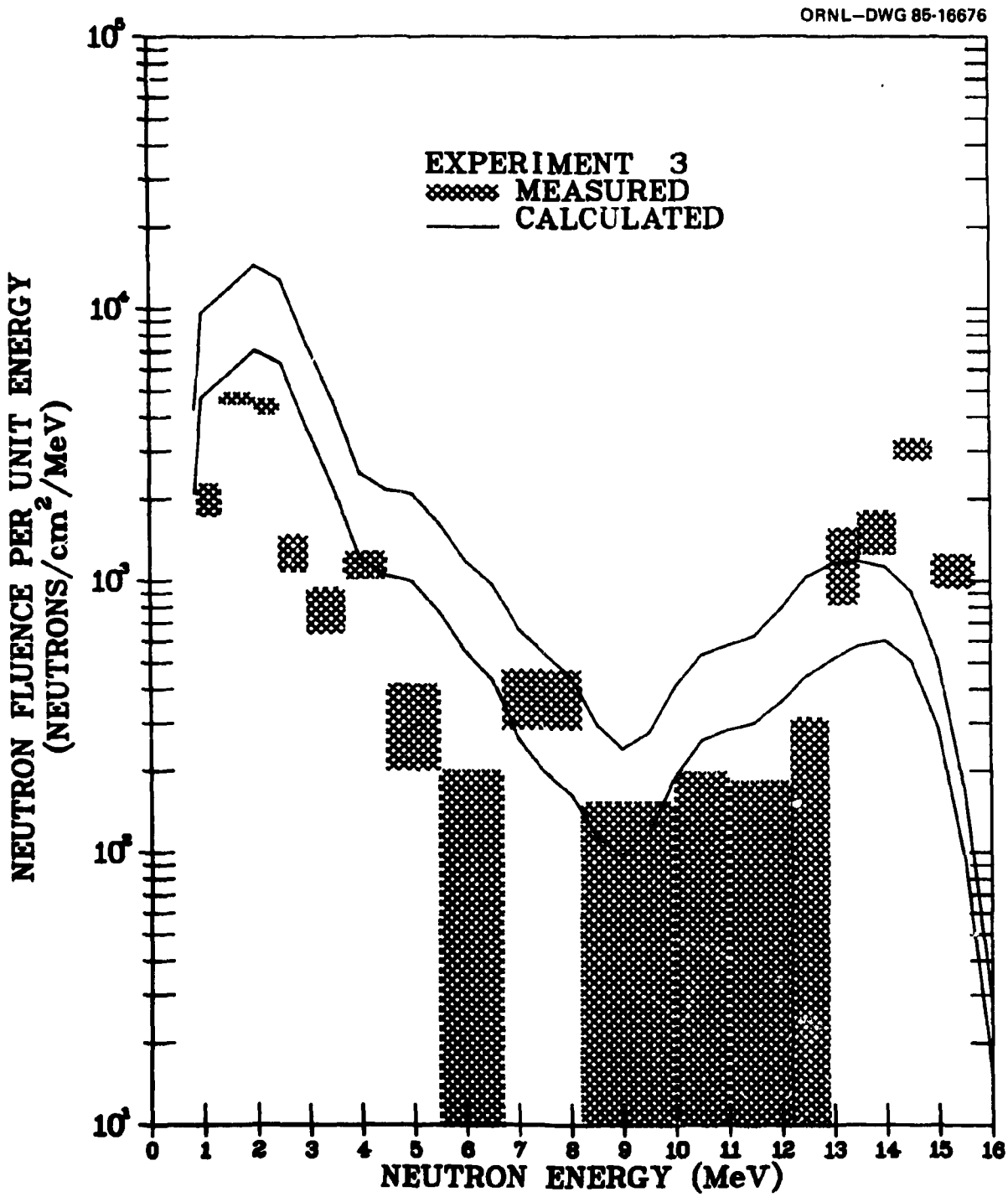

Fig. 5. Comparison of measured and calculated neutron fluences per unit energy for Exp. 3. The crosshatched regions indicate the 68% confidence intervals in the experimental measurements and the solid lines indicate the upper and lower bounds (± one standard deviation) due to the statistical error in the calculations.

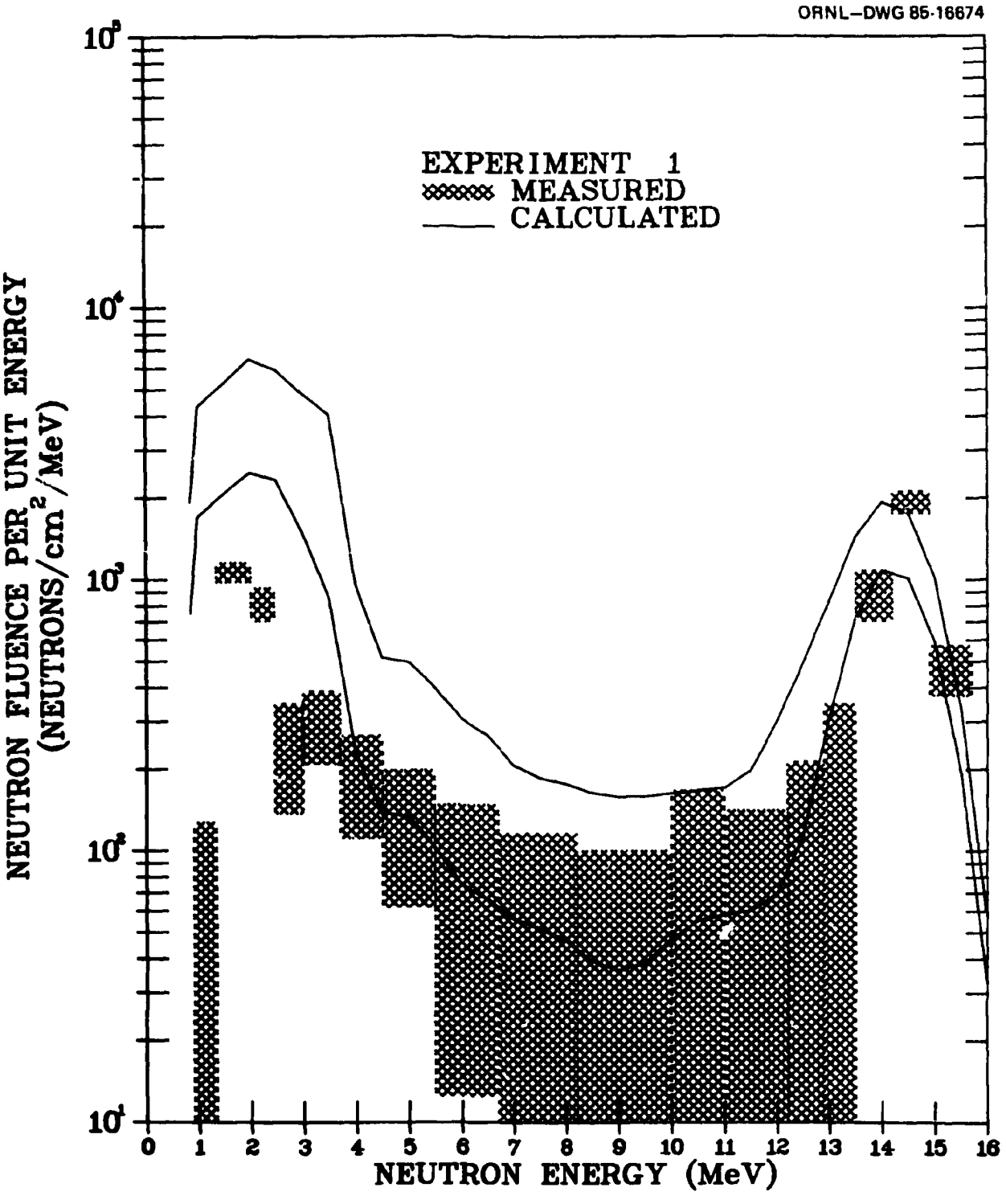

Fig. 6. Comparison of measured and calculated neutron fluences per unit energy for Exp. 1. The crosshatched regions indicate the 68% confidence intervals in the experimental measurements and the solid lines indicate the upper and lower bounds (± one standard deviation) due to the statistical error in the calculations .

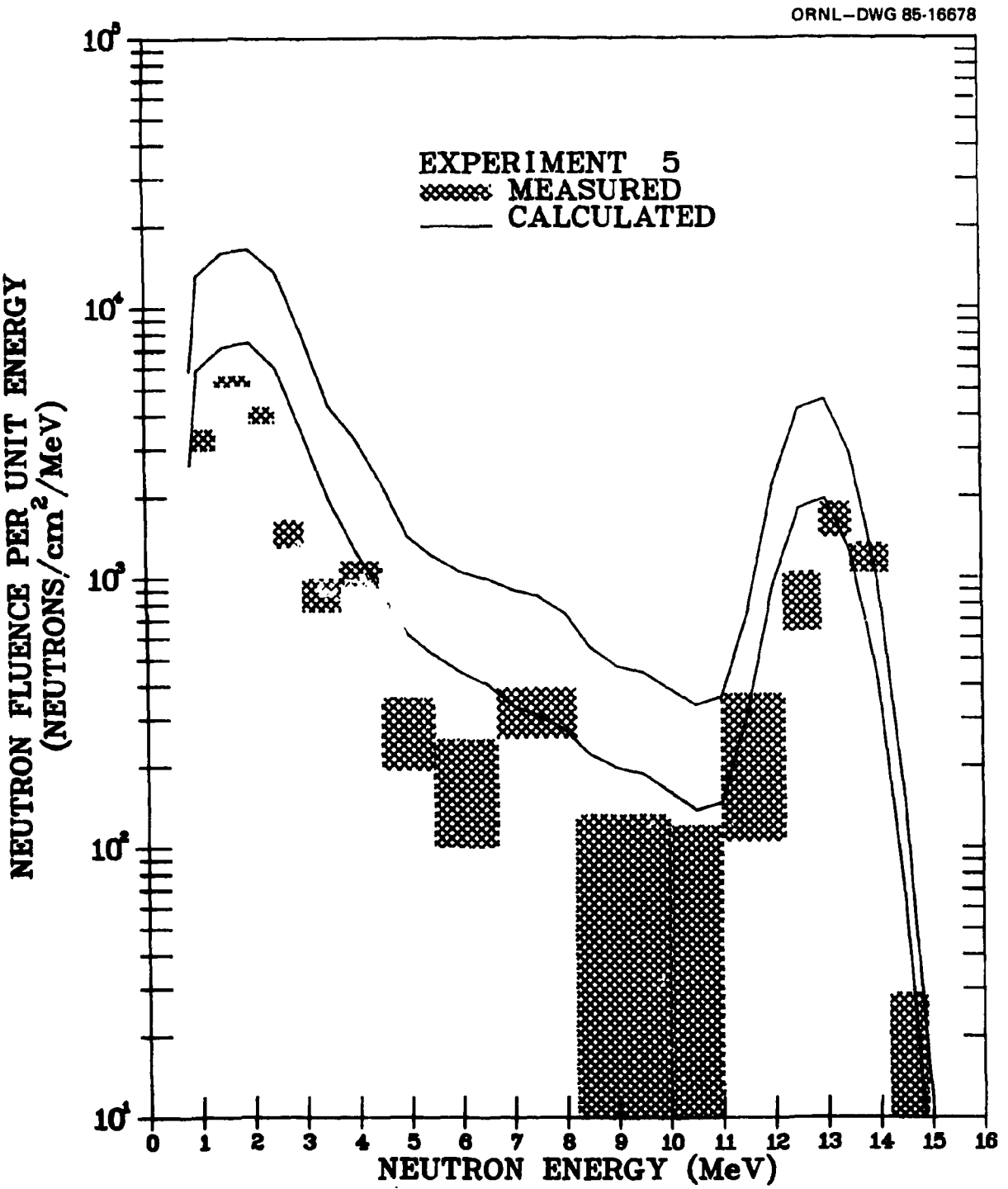

Fig. 7. Comparison of measured and calculated neutron fluences per unit energy for Exp. 5. The crosshatched regions indicate the 68% confidence intervals in the experimental measurements and the solid lines indicate the upper and lower bounds (± one standard deviation) due to the statistical error in the calculations .

For this reason, this experiment is thought to provide the greatest challenge to the calculational procedures. In Fig. 7 the calculated fluence per unit energy is somewhat larger than the measured fluence per unit energy at all energies. The calculated shape appears to be very similar to the experimental shape so in this case the differences appear to be primarily a difference in normalization. In Table 3 the ratio of the calculated to measured fluences is 2.9 $\pm$ 0.2, which is only slightly less than the ratio found in Exp. 5.

IV. SUMMARY

Calculated results have been compared with experimental data to determine the extent to which state-of-the-art neutron transport methods can be used to design the shielding for fusion reactors such as the TFTR. Substantial agreement has been obtained between the calculated and experimental fluences per unit energy for various combinations of source and detector positions. The calculated spectral shape is, in all cases, similar to the measured shape, but there are significant variations in the comparisons for different combinations of source and detector positions. In all cases considered the calculated fluence at energies $\geq$0.91 MeV are less than a factor of 4 larger than the measured fluence.

Full power D–T fusion experiments are not planned for some time in the future, but based on the results obtained here, it seems that one may have some confidence that the shielding requirements for such fusion reactor experiments can be reliably obtained using currently available state-of-the-art neutron transport methods.

REFERENCES

1. "Tokamak Fusion Test Reactor Final Design Report," PPPL-1475, Princeton Plasma Physics Laboratory, Princeton, NJ (1978).
2. J. K. Dickens et al., "Measurements of the Neutron and Gamma Ray Fluences in the TFTR Test Cell Due to a Point Source Simulating D-T Fusion Plasma Neutron Production," to be submitted for publication in *Nuclear Technology/Fusion.*
3. M. B. Emmett, "The MORSE Monte Carlo Radiation Transport System," ORNL-4744, Oak Ridge National Laboratory, Oak Ridge, TN (1975).
4. M. B. Emmett, L. M. Petrie, J. T. West, "JUNEBUG-II — A Three-Dimensional Geometry Plotting Code," NUREG/CR-0200, Vol. 2, Section F12, ORNL/NUREG-CSD-2/V2/R (December 1984).
5. Long-Poe Ku, "Nuclear Radiation Analysis for TFTR," PPPL-1711, Princeton Plasma Physics Laboratory, Princeton, NJ (1980).
6. R. T. Santoro, R. W. Roussin, and J. M. Barnes, "FLUNG: Coupled 35-Group Neutron and 21-Group Gamma Ray P_3 Cross Sections For Fusion Applications," ORNL/TM-7828, Oak Ridge National Laboratory, Oak Ridge, TN (1981).

ORNL/TM-9888
Distribution Category UC-20d

INTERNAL DISTRIBUTION

1–5. L. S. Abbott
6. F. S. Alsmiller
7–11. R. G. Alsmiller, Jr.
12–16. J. M. Barnes
17. L. A. Berry
18. D. G. Cacuci
19–23. J. D. Drischler
24–28. M. B. Emmett
29–31. EPD Reports Office
32. T. A. Gabriel
33. R. A. Lillie
34. J. L. Lucius
35. F. C. Maienschein
36. R. W. Peelle
37. R. W. Roussin
38. M. W. Rosenthal
39. RSIC
40–44. R. T. Santoro
45. T. E. Shannon
46. C. R. Weisbin
47. A. Zucker
48. P. W. Dickson, Jr. (Consultant)
49. G. H. Golub (Consultant)
50. R. Haralick (Consultant)
51. D. Steiner (Consultant)
52–53. Central Research Library
54. Fusion Energy Division Library
55. Fusion Energy Division Reports Office
56. ORNL Y-12 Technical Library Document Reference Section
57–58. Laboratory Records
59. ORNL Patent Office
60. Laboratory Records - RC

EXTERNAL DISTRIBUTION

61. Office of Assistant Manager for Energy Research & Development, DOE-ORO, Oak Ridge, TN 37830.

62. S. E. Berk, Division of Development and Technology, Office of Fusion Energy, ER-532, U.S. Dept. of Energy, Washington, DC. 20545.

63. J. D. Callen, Dept. of Nuclear Engineering, University of Wisconsin Madison, WI 53706.

64. R. W. Conn, Dept. of Chemical, Nuclear and Thermal Engineering, University of California, Los Angeles, CA 90024.

65. S. O. Dean, Director, Fusion Energy Development, Science Applications, Inc., 2 Professional Dr., Suite 249, Gaithersburg, MD 20760.

66. B. Engholm, General Atomic Co., P.O. Box 81608, San Diego, CA 92138.

67. H. K. Forsen, Bechtel Group, Inc., Research Engineering, P.O. Box 3964, San Francisco, CA 94105.

68. Y. Gohar, Argonne National Laboratory, 9700 S. Cass Avenue, Argonne, IL 60439

69. R. W. Gould, Dept. of Applied Physics, California Institute of Technology, Pasadena, CA 92024.

70. D. G. McAlees, Exxon Nuclear Co., Inc., 777 106th Ave., N.E., Bellevue, WA 98009.

71. Library, Princeton Plasma Physics Laboratory, Princeton University, P.O. Box 451, Princeton, NJ 08540.

72. P. Sager, General Atomic Co., P.O. Box 81608, San Diego, CA 92138.

73. W. M. Stacey, Jr., School of Nuclear Engineering, Georgia Institute of Technology, Atlanta, GA 30332.

EXTERNAL - FOREIGN

74. Bibliothek, Institut fur Plasmaphysik, D-8046, Garching bei Munchen, Federal Republic of Germany.

75. Bibliothek, Institut fur Plasmaphysik, KFA, Postfach 1913, D-5170, Julich 1, Federal Republic of Germany.

76. Bibliotheque, Service du Confinement des Plasmas, CEA, B.P. No. 6, 92, Fontenay aux Roses (Seine), France.

77. Documentation, S.I.G.N., D.P.PFC. CEN, P.O. 85, Centre de Tri, 38041 Cedex, Grenoble, France.

78. Institute of Physics, Academia Sinica, Peking, Peoples Republic of China.

79. Library, Centre de Recherches en Physique des Plasmas, 21 Avenue des Bains, 1007, Lausanne, Switzerland.

80. Library, Culham Laboratory, UKAEA, Abingdon, Oxon, OX14-3DB, England.

81. Library, FOM Institute voor Plasma-Fysica, Rijnhuizen, Jutphass, Netherlands.

82. Library, Institute for Plasma Physics, Nagoya University, Nagoya 464, Japan.

83. Library, International Centre for Theoretical Physics, Trieste, Italy.

84. Library, Laboratoria Gas Ionizzati, Frascati, Italy.
85. Library, Plasma Physics Laboratory, Kyoto University, Gokasho Uji, Kyoto, Japan.

86. Plasma Research Laboratory, Australian National University, P.O. Box 4, Canberra ACT.2000, Australia.

87. Dr. Yasushi Seki, Japan Atomic Energy Research Institute, Tokai-mura, Ibaraki-ken, Japan.

88. Thermonuclear Library, Japan Atomic Energy Research Institute, Tokai, Naka, Ibaraki, Japan.

89. R. Varma, Physical Research Laboratory, Navangpura, Ahmedabad, India.

90. Dr. Michinori Yamauchi, Nippon Atomic Industry Group Co., Ltd., NAIG Nuclear Research Laboratory, 4-1, Ukishima-cho, Kawasaki-ku, Kawasaki City, 210, Japan.

91–220. Given distribution as shown in TID-4500, Magnetic Fusion Energy (Distribution Category UC-20d: Fusion Systems).

Abstract

A recent paper presented neutron spectral distributions (energy ≥0.91 MeV) measured at various locations around the Tokamak Fusion Test Reactor (TFTR) at the Princeton Plasma Physics Laboratory. The neutron source for the series of measurements was a small D–T generator placed at various positions in the TFTR vacuum chamber. In the present paper the results of neutron transport calculations are presented and compared with these experimental data. The calculations were carried out using Monte Carlo methods and a very detailed model of the TFTR and the TFTR test cell. The calculated and experimental fluences per unit energy are compared in absolute units and are found to be in substantial agreement for five different combinations of source and detector positions.